Available online at www.sciencedirect.com
ScienceDirect
Trans. Nonferrous Met. Soc. China 26(2016) 1373−1378
Transactions of Nonferrous Metals Society of China
www.tnmsc.cn

Preparation and oxygen permeability of $Bi_{26}Mo_{10}O_{69}$ porous layer modified ionic-electronic mixed conductor on air side

Tai-he WANG[1], Rong LI[1], Qiang ZHEN[1,2], Lin CHENG[1]

1. Nano-Science and Technology Research Center, Shanghai University, Shanghai 200444, China;
2. School of Materials Science and Engineering, Shanghai University, Shanghai 200072, China

Received 6 May 2015; accepted 17 November 2015

Abstract: $Bi_{26}Mo_{10}O_{69}$ nanopowder was prepared by hydrothermal method and used as a surface modification material for oxygen separation membrane to enhance oxygen permeability. Thermal decomposition behavior and phase variation of the precursor were investigated by thermal analyzer (TG-DSC) and high-temperature X-ray diffraction (HT-XRD). $Bi_{26}Mo_{10}O_{69}$ porous layer was coated on the air side of $BaCo_{0.7}Fe_{0.2}Nb_{0.1}O_{3-\delta}$ (BCFN) oxygen permeable membrane by dipping method. In the partial oxidation experiment of coke oven gas (COG), the $Bi_{26}Mo_{10}O_{69}$-coated BCFN membrane exhibits higher oxygen permeability and CH_4 conversion than the uncoated BCFN membrane. When the thickness of BCFN membrane was 1 mm and the COG and air fluxes were 120 and 100 mL/min, the oxygen permeation flux reached 16.48 mL/(min·cm^2) at 875 °C, which was 16.96% higher than the uncoated BCFN membrane. Therefore, $Bi_{26}Mo_{10}O_{69}$ porous layer on the air side will be promising modification coating on the oxygen permeability of BCFN membrane.

Key words: $Bi_{26}Mo_{10}O_{69}$; porous-coating; $BaCo_{0.7}Fe_{0.2}Nb_{0.1}O_{3-\delta}$(BCFN); oxygen permeation flux

1 Introduction

Mixed ionic and electronic conductors are considered as promising materials for partial oxidation of methane (POM) to synthesize syngas (H_2−CO mixture) [1]. Pervoskite-type oxides (ABO_3), such as $SrCo_{0.8}Fe_{0.2}O_{3-\delta}$ (SCF) [2], $Ba_{1-x}Sr_xCo_{0.8}Fe_{0.2}O_{3-\delta}$ (BSCF) [3] and $La_{1-x}Sr_xFe_{1-y}M_yO_{3-\delta}$ (LSFM) [4,5], display infinite oxygen selectivity from air and higher oxygen fluxes compared with other organic membranes [6,7]. Among these materials, $BaCo_{0.7}Fe_{0.2}Nb_{0.1}O_{3-\delta}$ (BCFN) shows high oxygen permeability and better chemical stability under reducing atmosphere in oxygen permeation process [8,9]. It is reported that BCFN with thickness of 1 mm shows an oxygen permeation flux of 1.63 mL/(min·cm^2) at 875 °C [10]. However, this value is still not high enough to satisfy the requirement for industrial application.

When the oxygen permeation is limited by bulk diffusion, decreasing the thickness of the membrane could enhance the permeation rate, but it will also lead to low mechanical strength. And for a thin membrane ($L \leq L_c$, L_c is defined as the thickness of membrane that divides the bulk limit and surface limit), oxygen surface exchange rate will become a dominant factor for oxygen permeability [11,12]. Thus, surface modification is usually an effective technique to further increase the oxygen permeability. It was reported that for $Ba_{0.5}Sr_{0.5}Co_{0.8}Fe_{0.2}O_{3-\delta}$ membrane with a single $GdBaCo_2O_{5+\delta}$ layer on the helium side, the oxygen permeation flux could rise by 23% at 875 °C [13]. CHENG et al [14] reported that BCFN membrane coated with $Ce_{0.8}Re_{0.2}O_{2-\delta}$ (Re=Sm, Gd) porous layer on the reductive side showed significant enhancement in oxygen permeation flux.

However, oxygen permeability is also improved by coating porous layer on air side of membrane [15,16]. SHEN et al [17] proposed that on air side of the membrane, if the coating layer had a faster oxygen adsorption rate constant than the membrane material, oxygen ions could accumulate in the coating layer, thus a

Foundation item: Projects (51272154, 51472156) supported by the National Natural Science Foundation of China; Projects (sdcx2012033, sdcx2012062) supported by the Innovation Fund of Shanghai University, China; Project (14ZR1416400) supported by Special Research Foundation for Training and Selecting Outstanding Young Teachers of Universities in Shanghai, China; Project supported by Shanghai Science and Technology Committee, China

Corresponding author: Rong LI; Tel: +86-21-66137266; E-mail: li-rong@shu.edu.cn

DOI: 10.1016/S1003-6326(16)64241-3

higher oxygen pressure could be formed on the surface and resulted in higher oxygen permeation flux. HONG et al [18] investigated $La_{0.6}Sr_{0.4}Co_{0.8}Fe_{0.2}O_{3-\delta}$ (LSCF) dense ceramic with porous $Sm_xCe_{1-x}O_{2-\delta}$ layer and found obvious effects on surface exchange rate. The surface exchange coefficient increased almost linearly with ionic conductivity of $Sm_xCe_{1-x}O_{2-\delta}$, since the $Sm_xCe_{1-x}O_{2-\delta}$ supplied additional free oxygen vacancies, which is critical for oxygen incorporation in LSCF. Therefore, high ionic conductivity and oxygen adsorption ability are expected for a porous layer on the oxygen membrane.

Recently, most research has focused on perovskite oxide and fluorite structure oxides, such as CeO_2-based material as porous layer. Compared with these materials, Bi_2O_3-based materials exhibit higher ionic conductivity. The binary oxide $Bi_{26}Mo_{10}O_{69}$ is a new family of oxygen ion conductors, and this type of compound displays a transference number almost unity for the oxygen ions in air [19,20]. However, $Bi_{26}Mo_{10}O_{69}$ was usually synthesized by solid reaction method with micron grain size. In this work, $Bi_{26}Mo_{10}O_{69}$ nanopowder was successfully prepared by hydrothermal method, and the decomposition behavior of precursor was also investigated by TG-DSC and high-temperature XRD (HT-XRD). The oxygen permeation flux was studied in partial oxidation experiment of coke oven gas (COG) with submicron $Bi_{26}Mo_{10}O_{69}$ porous layer coated on the air side of BCFN dense membrane.

2 Experimental

2.1 Sample preparation

Using analytically pure Bi_2O_3 and $(NH_4)_6Mo_7O_{24}\cdot 4H_2O$ agents as raw materials, $Bi_{26}Mo_{10}O_{69}$ precursor was synthesized by hydrothermal method. Bi_2O_3 was dissolved in a nitric acid with Bi^{3+} concentration of 1.7 mol/L, while $(NH_4)_6Mo_7O_{24}\cdot 4H_2O$ was dissolved in an ammonia solution with Mo^{3+} concentration of 0.9 mol/L. Then, the nitrate solution was dropwise added into the ammonia solution with continuous stirring, and the pH value of this mixed solution was controlled at 7. The mixed solution was poured into hydro-thermal reactor and kept at 180 °C for 20 h. After being filtered and dried at 80 °C, the precursor was calcined at 800 °C for 3 h to obtain $Bi_{26}Mo_{10}O_{69}$ nanopowders.

BCFN dense membrane with a thickness of 1 mm was prepared according to Ref. [14]. The slurry, a mixture of $Bi_{26}Mo_{10}O_{69}$ nanopowder, terpineol, carbon fiber, ethyl cellulose and polyethylene glycol, was coated on the air side of BCFN membranes by dipping method. The coated samples were heated at 600 °C for 3 h with a heating rate of 5 °C/min.

2.2 Characterization

Thermal decomposition behavior of $Bi_{26}Mo_{10}O_{69}$ precursor was investigated using composite thermal analyzer (STA409PC, Germany). The experiment was carried out in air from room temperature to 950 °C with a heat rate of 10 °C/min [19].

A D8 advance AXS Bruker diffractometer (Cu K_α radiation, Germany), equipped with a HTK 1200N Anton Paar high temperature chamber, was used to study the phase variation of the $Bi_{26}Mo_{10}O_{69}$ precursor during the heating process from room temperature to 925 °C. The diagrams were collected every 20 °C, in the $20°\leq 2\theta \leq 80°$ domain, with a 0.0148° step size and a counting time of 0.2 s per step.

Phases of $Bi_{26}Mo_{10}O_{69}$ nanopowder and $Bi_{26}Mo_{10}O_{69}$ coated BCFN membrane were characterized by X-ray diffraction (Rigaku, D/max−2550, Japan) in the range of $20°\leq 2\theta \leq 80°$, with a 0.02° step size and a 4 (°)/min scanning rate. The average crystalline size of $Bi_{26}Mo_{10}O_{69}$ nanopowder was calculated using the Scherrer equation $D=0.89\lambda/(B\cos\theta)$, where B is the full width at half maximum of Bragg peaks.

Micrograph of $Bi_{26}Mo_{10}O_{69}$ nanopowder was observed using transmission electron microscopy (JEOL, 200CX, Japan). The microstructure of surface and cross section of $Bi_{26}Mo_{10}O_{69}$ coated BCFN sample was observed by scanning electron microscopy (JEOL, 6700F, Japan).

2.3 Oxygen permeation experiment

The permeation properties of the disk shape membranes were investigated in vertical high temperature oxygen permeation apparatus, as shown in Fig. 1. The membrane (d=17 mm, t=1 mm) was sealed with sliver rings to quartz tubes on both sides, and the effective area of membrane exposed to gas was 1.3 cm^2. In the experiment, a total of 1.0 g of 0.4−0.8 mm $Co_{0.3}Mg_{0.7}O$ powder was directly placed on the upper

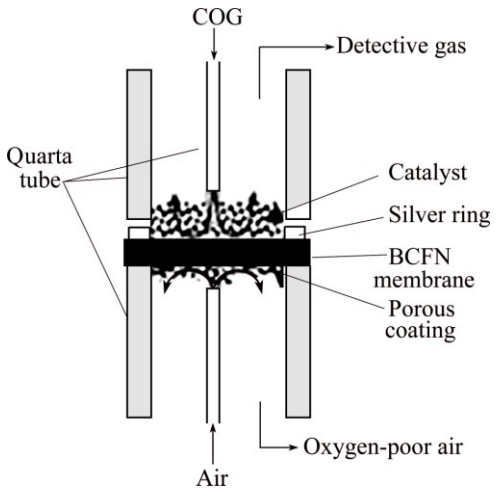

Fig. 1 Schematic of membrane reactor for oxygen permeation

surface of membrane as catalyst. COG (31.8% CH_4, 57.705% H_2, 7.366% CO and 3.069% O_2) and the air passed through two quartz inner tubes to sweep the upper and lower surfaces of the membrane, respectively. The gas flow rates were controlled by mass flow controllers.

Prior to the experiment, gas-tightness of membrane reactor was examined by detecting nitrogen in the outlet gas. On the permeation side of the membrane, the water was removed by $Mg(ClO_4)_2$, and H_2, CO, CO_2 and CH_4 in the outlet gas were analyzed by a Varian CP3800 gas chromatography (GC) with a thermal conductivity detector (TCD). According to the law of mass conservation, the oxygen permeation flux, CH_4 conversion and H_2 selectivity were calculated from H_2, CO, CO_2 and CH_4 concentrations and the flow rate of the inlet and outlet gas [14,21].

3 Results and discussion

3.1 Thermal decomposition behavior of $Bi_{26}Mo_{10}O_{69}$ precursor

Figure 2 shows the TG-DSC curves of $Bi_{26}Mo_{10}O_{69}$ precursor obtained by hydrothermal method. Before 480 °C, the mass loss of 2.7% was mainly caused by the release of adsorbed water and the burning of organic disperser, then by the decomposition of the small amount of hydroxide, corresponding to an endothermic peak at 430 °C. After 480 °C, the TG curve tends to be plat, no mass loss was observed. However, an endothermic peak occurred at 710 °C in the DSC curve caused by the phase variation.

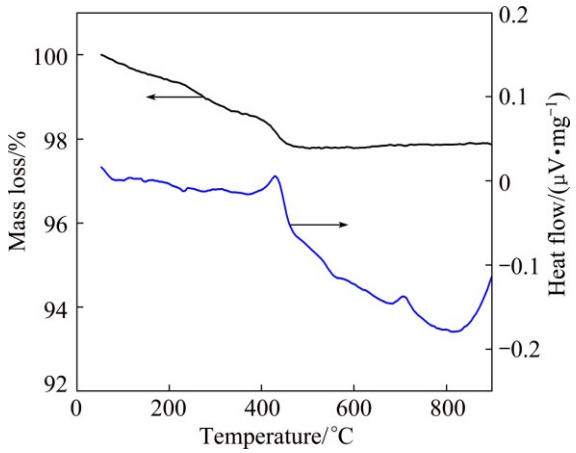

Fig. 2 TG-DSC curves of $Bi_{26}Mo_{10}O_{69}$ precursor in heating process

The precursor was also studied by HT-XRD and the diffractograms are shown in Fig. 3. Orthorhombic phase Bi_2MoO_6 and cubic phase Bi_2O_3 were identified from room temperature to 440 °C. At 440 °C, the peaks of Bi_2MoO_6 and Bi_2O_3 started to change into a new phase. The disappearance of Bi_2MoO_6 was observed at 700 °C, and it was replaced by a monoclinic phase of $Bi_{26}Mo_{10}O_{69}$. This phase variation was also observed in DSC curve with an endothermic peak at 710 °C. At 800 °C, only monoclinic $Bi_{26}Mo_{10}O_{69}$ was observed, and this phase structure was kept when returned to room temperature.

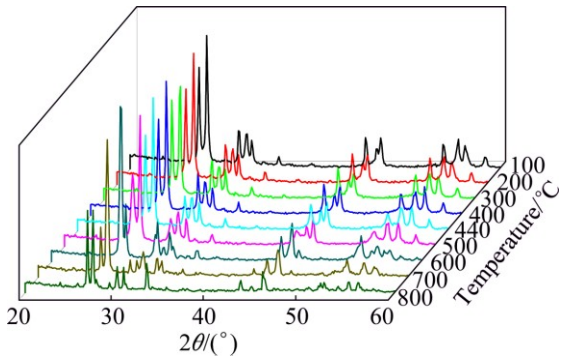

Fig. 3 High temperature X-ray diffraction patterns of $Bi_{26}Mo_{10}O_{69}$ precursor

3.2 Characterization of $Bi_{26}Mo_{10}O_{69}$ nanopowder

According to the results of TG-DSC and HT-XRD, the precursor was calcined at 800 °C for 3 h to obtain $Bi_{26}Mo_{10}O_{69}$ nanopowder. Figure 4(a) gives the XRD pattern of $Bi_{26}Mo_{10}O_{69}$ nanopowder, as expected from

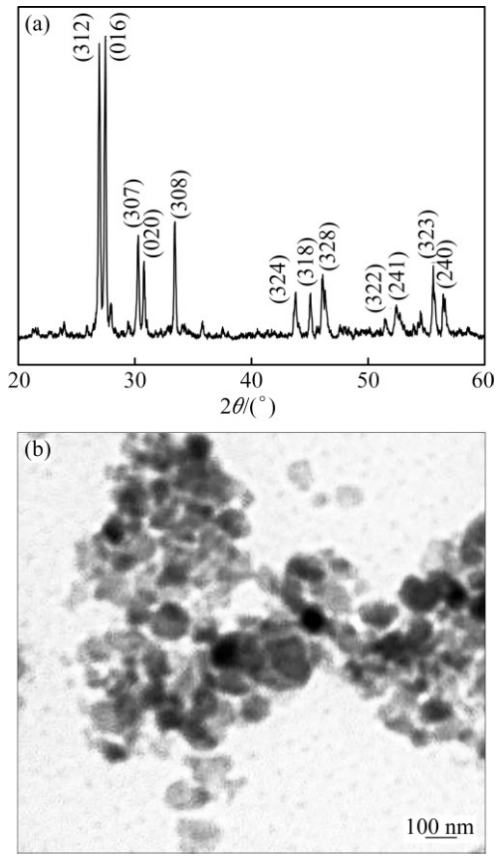

Fig. 4 XRD pattern (a) and TEM image (b) of $Bi_{26}Mo_{10}O_{69}$ nanopowder

high temperature XRD, pure $Bi_{26}Mo_{10}O_{69}$ phase was obtained. Calculated by the Scherrer equation, the average grain size was 70 nm. The TEM image of $Bi_{26}Mo_{10}O_{69}$ nanopowder is shown in Fig. 4(b). It shows that the particles are nearly spherical shape with grain size smaller than 100 nm, which is in good agreement with the calculated value from XRD.

3.3 Characterization of $Bi_{26}Mo_{10}O_{69}$ porous layer coated BCFN membrane

Figure 5 shows the XRD patterns of $Bi_{26}Mo_{10}O_{69}$-coated BCFN and BCFN membranes, respectively. The BCFN membrane exhibits a cubic pervoskite structure. For $Bi_{26}Mo_{10}O_{69}$-coated BCFN sample, the main peaks correspond to both $Bi_{26}Mo_{10}O_{69}$ and pervoskite structure, and no impurity phase is observed, revealing that the coexistence of the BCFN and $Bi_{26}Mo_{10}O_{69}$ is stable.

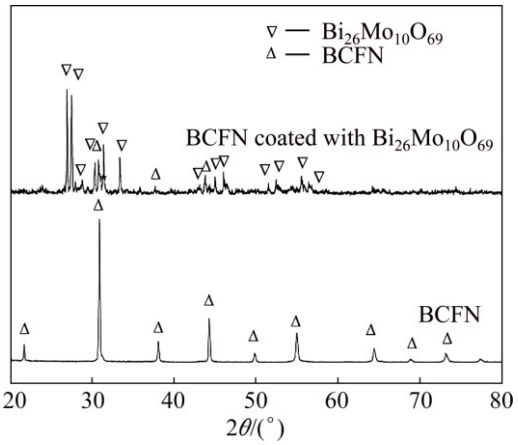

Fig. 5 XRD patterns of $Bi_{26}Mo_{10}O_{69}$ coated BCFN and uncoated BCFN membrane

Figure 6 shows the microstructures of the surface and the cross section of $Bi_{26}Mo_{10}O_{69}$-coated BCFN sample. From Fig. 6(a), $Bi_{26}Mo_{10}O_{69}$ coating layer exhibits a porous structure, caused by the volatilization of the organic solution in the slurry. From Fig. 6(b), it can be seen that $Bi_{26}Mo_{10}O_{69}$ porous layer tightly contacts with BCFN membrane, and the thickness of porous layer is about 5 μm.

3.4 Oxygen permeability of $Bi_{26}Mo_{10}O_{69}$-coated BCFN membrane

Figure 7 presents the oxygen permeation flux (J_{O_2}) of $Bi_{26}Mo_{10}O_{69}$-coated BCFN and uncoated BCFN membranes at 875 °C as a function of COG flow rate. The flow rate of air is 100 mL/min. The oxygen permeation flux increases with rising COG flow rate, which could be attributed to the lower oxygen partial pressure on the permeation side. $Bi_{26}Mo_{10}O_{69}$-coated BCFN exhibits higher oxygen permeation flux than uncoated BCFN membrane. When the COG flux was

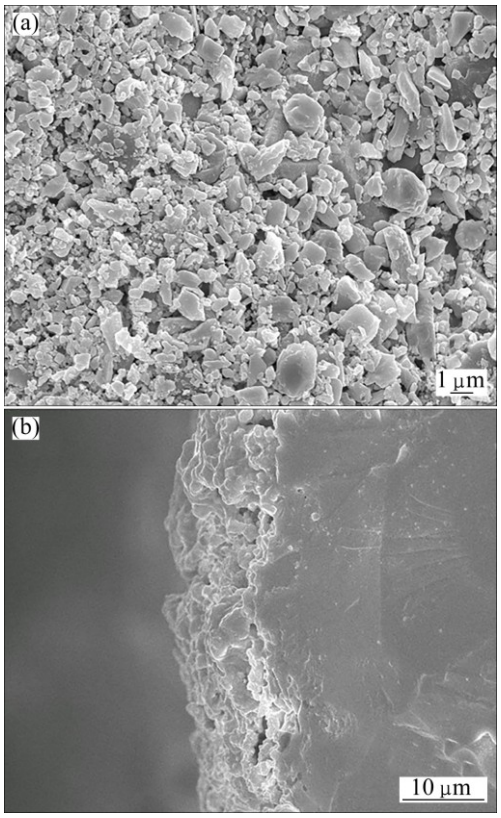

Fig. 6 SEM images of $Bi_{26}Mo_{10}O_{69}$ coated BCFN membrane

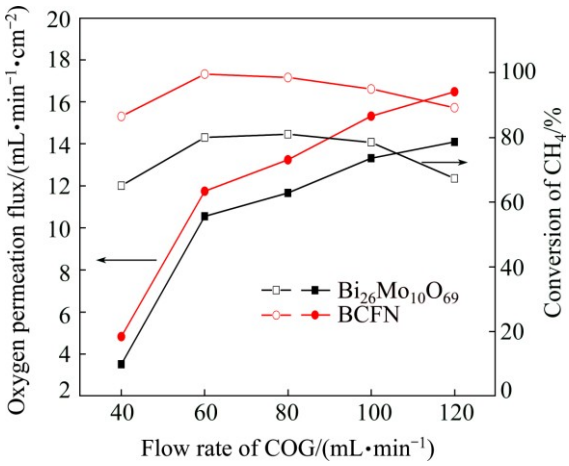

Fig. 7 Oxygen permeation flux and CH_4 conversion of $Bi_{26}Mo_{10}O_{69}$-coated BCFN and uncoated BCFN membrane (Reaction conditions: COG flow rate, 40−120 mL/min; air flow rate, 100 mL/min; membrane thickness, 1.0 mm; temperature, 875 °C)

120 mL/min, the oxygen permeation flux of $Bi_{26}Mo_{10}O_{69}$ coated BCFN reached 16.48 mL/(min·cm^2), which was 16.96% higher than that of the uncoated BCFN membrane. The CH_4 conversion of BCFN membrane with and without $Bi_{26}Mo_{10}O_{69}$ coating is shown in Fig. 7. It can be seen that the $Bi_{26}Mo_{10}O_{69}$-coated BCFN membrane showed significant enhancement in CH_4 conversion. The average growth was 19.4%. When the

COG flux was 60 mL/min, the CH_4 conversion of $Bi_{26}Mo_{10}O_{69}$-coated BCFN reached 99.6%, while that of the uncoated BCFN membrane was only 80%. At the meantime, the H_2 selectivities were 79.6% and 59%, respectively.

The improvement in oxygen permeation flux on one hand relies on the extra surface area and active sites arising from the nanoparticles, on the other hand is owing to the coating layer, which may change the effective oxygen pressure on the surface of the membrane [14]. Therefore, the porous coating could accurate the process of oxygen reduction process.

4 Conclusions

1) $Bi_{26}Mo_{10}O_{69}$ precursor was prepared by hydrothermal method. Thermal decomposition behavior of the precursor was investigated by TG-DSC and high-temperature X-ray diffractometry, and Bi_2O_3, Bi_2MoO_6 were found in the precursor.

2) With temperature increasing, Bi_2O_3 and Bi_2MoO_6 started to form a new phase, Bi_2MoO_6 disappeared at 700 °C, and monoclinic phase of $Bi_{26}Mo_{10}O_{69}$ was observed at 800 °C. After calcining the precursor at 800 °C for 3 h, $Bi_{26}Mo_{10}O_{69}$ nanopowder with grain size of 70 nm was obtained.

3) $Bi_{26}Mo_{10}O_{69}$ porous layer was coated on the air side of BCFN membrane by dipping method, and no reaction between BCFN and coating layer was observed.

4) In the partial oxidation experiment of COG, the $Bi_{26}Mo_{10}O_{69}$-coated BCFN exhibits higher oxygen permeability than uncoated BCFN. When the COG flux and air flux were 120 mL/min and 100 mL/min, the oxygen permeation flux reached 16.48 mL/(min·cm^2), which was 16.96% higher than uncoated BCFN membrane. This means that $Bi_{26}Mo_{10}O_{69}$ porous layer on the air side can improve the oxygen permeability of ionic-electronic mixed conductor. However, the improving mechanism in oxygen permeation needs to be further studied.

References

[1] DU Yun-peng, ZHU Xing, WANG Hua, WEI Yong-gang, LI Kong-zhai. Selective oxidation of methane to syngas using $Pr_{0.7}Zr_{0.3}O_{3-\delta}$: Stability of oxygen carrier [J]. Transactions of Nonferrous Metals Society of China, 2015, 25(4): 1248−1253.

[2] KLANDE T, RAVKINA O, FELDHOFF A. Effect of microstructure on oxygen permeation of $Ba_{0.5}Sr_{0.5}Co_{0.8}Fe_{0.2}O_{3-\delta}$ and $SrCo_{0.8}Fe_{0.2}O_{3-\delta}$ membranes [J]. Journal of the European Ceramic Society, 2013, 33(6): 1129−1136.

[3] BAUMANN S, SERRA J M, LOBERA M P, ESCOLÁSTICO S, SCHULZE-KUPPERS F, MEULENBERG W A. Ultrahigh oxygen permeation flux through supported $Ba_{0.5}Sr_{0.5}Co_{0.8}Fe_{0.2}O_{3-\delta}$ membranes [J]. Journal of Membrane Science, 2011, 377(1): 198−205.

[4] GURAUSKIS J, LOHNE Ø F, WIIK K. $La_{0.2}Sr_{0.8}Fe_{0.8}Ta_{0.2}O_{3-\delta}$ based thin film membranes with surface modification for oxygen production [J]. Solid State Ionics, 2012, 225: 703−706.

[5] GEFFROY P M, VIVET A, NGUYEN L, BLOND E, RICHET N, CHARTIER T. Elaboration of $La_{1-x}Sr_xFe_{1-y}Ga_yO_{3-\delta}$ multilayer membranes by tape casting and co-firing for syngas application [J]. Journal of the European Ceramic Society, 2013, 33(10): 1849−1858.

[6] ZHOU Chao, XIA Si-qing, GAO Nai-yun, CHU Wen-hai. Recycling of bath wastewater treated by membrane bioreactor [J]. Journal of Central South University, 2012, 43: 1999−2003. (in Chinese)

[7] REN Xiu-lian, WEI Qi-feng, LIU Zhe, LIU Jun. Electrodeposition conditions of metallic nickel in electrolytic membrane reactor [J]. Transactions of Nonferrous Metals Society of China, 2012, 22(2): 467−475.

[8] HARADA M, DOMEN K, HARA M, TATSUMI T. $Ba_{1.0}Co_{0.7}Fe_{0.2}Nb_{0.1}O_{3-\delta}$ dense ceramic as an oxygen permeable membrane for partial oxidation of methane to synthesis gas [J]. Chemistry Letters, 2006, 35(12): 1326−1327.

[9] CHENG Yun-fei, ZHAO Hai-lei, TENG De-qiang, LI Fu-shen, LU Xiong-gang, DING Wei-zhong. Investigation of Ba fully occupied A-site $BaCo_{0.7}Fe_{0.3-x}Nb_xO_{3-\delta}$ perovskite stabilized by low concentration of Nb for oxygen permeation membrane [J]. Journal of Membrane Science, 2008, 322(2): 484−490.

[10] YANG Zhi-bin, DING Wei-zhong, ZHANG Yun-yan, LU Xiong-gang, ZHANG Yu-wen, SHEN Pei-jun. Catalytic partial oxidation of coke oven gas to syngas in an oxygen permeation membrane reactor combined with NiO/MgO catalyst [J]. International Journal of Hydrogen Energy, 2010, 35(12): 6239−6247.

[11] BOUWMEESTER H M, KRUIDHOF H, BURGGRAAF A J. Importance of the surface exchange kinetics as rate limiting step in oxygen permeation through mixed-conducting oxides [J]. Solid State Ionics, 1994, 72: 185−194.

[12] HONG W K, CHOI G M. Oxygen permeation of BSCF membrane with varying thickness and surface coating [J]. Journal of Membrane Science, 2010, 346(2): 353−360.

[13] WANG Ying-fang, HAO Hao-shan, JIA Jian-feng, YANG De-lin, HU Xing. Improving the oxygen permeability of $Ba_{0.5}Sr_{0.5}Co_{0.8}Fe_{0.2}O_{3-\delta}$ membranes by a surface-coating layer of $GdBaCo_2O_{5+\delta}$ [J]. Journal of the European Ceramic Society, 2008, 28(16): 3125−3130.

[14] CHENG Hong-wei, LU Xiong-gang, HU Da-hai, ZHANG Yu-wen, DING Wei-zhong, ZHAO Hai-lei. Hydrogen production by catalytic partial oxidation of coke oven gas in $BaCo_{0.7}Fe_{0.2}Nb_{0.1}O_{3-\delta}$ membranes with surface modification [J]. International Journal of Hydrogen Energy, 2011, 36(1): 528−538.

[15] PAN Hai-ping, LI Li-ping, DENG Xin, MENG Bo, TAN Xiao-yao, LI K. Improvement of oxygen permeation in perovskite hollow fibre membranes by the enhanced surface exchange kinetics [J]. Journal of Membrane Science, 2013, 428: 198−204.

[16] CHEN Ting, ZHAO Hai-lei, XIE Zhi-xiang, FENG Lin-chang, LU Xiong-gang, DING Wei-zhong, LI Fu-shen. Electrical conductivity and oxygen permeability of $Ce_{0.8}Sm_{0.2}O_{2-\delta}$–$PrBaCo_2O_{5+\delta}$ dual-phase composites [J]. International Journal of Hydrogen Energy, 2012, 37(6): 5277−5285.

[17] SHEN Zi-gang, LU Peng-xian, YAN Gang, HU Xing. Enhancing the oxygen permeability of $Ba_{0.5}Sr_{0.5}Co_{0.8}Fe_{0.2}O_{5+\delta}$ membranes by coating $RBaCo_2O_{5+\delta}$ (R= Pr, Nd, Sm, Gd) layers [J]. Materials Letters, 2010, 64(8): 980−982.

[18] HONG Tao, ZHANG Lei, CHEN Fang-lin, XIA Chang-rong. Oxygen surface exchange properties of $La_{0.6}Sr_{0.4}Co_{0.8}Fe_{0.2}O_{3-\delta}$ coated with $Sm_xCe_{1-x}O_{2-\delta}$ [J]. Journal of Power Sources, 2012, 218: 254−260.

[19] VANNIER R N, MAIRESSE G, ABRAHAM F, NOWOGROCKI G. $Bi_{26}Mo_{10}O_\delta$ solid solution type in the Bi_2O_3–MoO_3–V_2O_5 ternary diagram [J]. Journal of Solid State Chemistry, 1996, 122(2):

394−406.

[20] FAFILEK G, KUREK P. Electrochemical stability studies by voltammetry on microsamples based on $Bi_{26}Mo_{10}O_{69}$ [J]. Solid State Ionics, 2003, 157(1): 171−176.

[21] YUAN Qiang, ZHEN Qiang, LI Rong. Preparation and oxygen permeability of $BaCo_{0.7}Fe_{0.2}Nb_{0.1}O_{3-\delta}$ membrane modified by $Ce_{0.8}Y_{0.2}O_{3-\delta}$ porous layer on the air side [J]. Journal of Nanomaterials, 2013(157474): 1−6.

$Bi_{26}Mo_{10}O_{69}$ 多孔涂层空气侧改性混合离子导体的制备及其增进透氧性能

王太和[1]，李 榕[1]，甄 强[1,2]，程 琳[1]

1. 上海大学 纳米科学与技术研究中心，上海 200444；
2. 上海大学 材料科学与工程学院，上海 200072

摘 要：通过水热法合成 $Bi_{26}Mo_{10}O_{69}$ 纳米粉体，并作为表面改性材料用于提高氧分离膜的透氧性能。通过 TG−DSC 和高温 XRD(HT-XRD)对前驱体的热分解行为及物相变化进行研究。采用浸渍法在 $BaCo_{0.7}Fe_{0.2}Nb_{0.1}O_{3-\delta}$ (BCFN)的空气侧涂覆 $Bi_{26}Mo_{10}O_{69}$ 多孔涂层。在焦炉煤气(COG)的部分氧化重整实验中，涂覆 $Bi_{26}Mo_{10}O_{69}$ 多孔涂层的 BCFN 膜的透氧量和 CH_4 转化率均高于无涂层的 BCFN 膜。当 BCFN 透氧膜厚度为 1mm，COG 流量和空气流量分别为 120 mL/min 和 100 mL/min 时，875 °C 透氧速率达到 16.48 mL/(min·cm^2)，比无涂层的 BCFN 膜高 16.96%。因此，空气侧 $Bi_{26}Mo_{10}O_{69}$ 多孔涂层有望作为改性涂层提高 BCFN 膜的透氧性能。

关键词：$Bi_{26}Mo_{10}O_{69}$；多孔涂层；$BaCo_{0.7}Fe_{0.2}Nb_{0.1}O_{3-\delta}$(BCFN)；透氧速率

(Edited by Xiang-qun LI)